PCCP

Accepted Manuscript

ROYAL SOCIETY OF CHEMISTRY

www.rsc.org/pccp

ARTICLE TYPE www. rsc.org/xxxxxx | XXXXXXXX

Model Atomistic Protrusions Favouring Ordering and Retention of Water†

Prithvi Raj Pandey*[a] and Sudip Roy[a]

Received Xth XXXXXXXXXX 20XX, Accepted Xth XXXXXXXXX 20XX
First published on the web Xth XXXXXXXXXX 2014
DOI: 10.1039/b000000x

Ordering of water molecules near model linear atomistic protrusions is studied using classical molecular dynamics simulations. The protrusions are made up of Lennard-Jones particles of hydrophobic and hydrophilic blocks. Simulations are performed at a range of temperatures and pressures keeping the protrusions position restrained. At different temperature and pressure ordering and residence time of water molecules get enhances on the surface of hydrophilic block. Detailed analysis of the systems show that surface region is potentially most favorable energetically for water molecules, which is consistent with the tetrahedral ordering of water molecules. A competition between energetics and structuring is observed from the residence time calculations.

1 Introduction

Water is the most abundant solvent on earth. Water is present as bulk, as well as in confined regions with different structural arrangement than bulk. Water inside confined regions has drawn significant amount of research attention in the recent past[1,2]. Confined water is structurally different and show properties not similar to bulk[3]. The importance, and characteristics of confined water has been envisaged in varied range of systems. Biological systems (protein grooves, cell membranes)[4,5], nanostructured materials[6,7], geological systems[8] have been studied experimentally and theoretically with the motivation to understand the structure and dynamics of water present under confinement. In addition to structure and dynamics, phase behavior of water inside confined regions were also studied in the past[9]. This is because confinement is capable of inducing melting-freezing, wetting-drying transitions, and also prewetting and predrying transitions (reference[9] and references therein). The effect of confinement of water on its structuring has been discussed by Mancinelli[2].

Molecular dynamics (MD) simulations have been used extensively in understanding of molecular level structure and dynamics of water inside confined regions. Phase behavior of water confined inside hydrophobic surfaces was studied by using MD simulations by Koga et al[9]. They have analyzed the structural, and thermodynamical aspects of water inside the hydrophobic surfaces. Johnston et al. have studied the phase behavior of water inside Lennard-Jones (LJ) 9-3 walls[10]. Phase diagram of water was investigated inside carbon nanoube (CNT) by Takaiwa et al. as a function of diameter of the tube[3]. Khan et al. have studied wetting of textured surfaces by nanodroplets using MD simulations[11]. Rotational entropy of water inside CNT was studied by Kumar et al.[12]. Lombardo et al. have investigated the mechanical and structural properties of glassy water confined inside atomistic silica based surfaces[13]. Bauer et al. have studied the effect of confined water on the energetics of assembly of large hydrophobic plates[14]. All these studies are performed either in model systems or in nano-structured materials and collectively explained the structural, and thermodynamical properties of confined water. These properties are expected to be tunable by changing the parameters (hydrophobicity, roughness, dimension and volume of confinement) of the model systems or changing the pattern and chemical constituent of the nanostructured materials. Changing chemical constituent can be resembled with changing hydrophobic or hydrophilic strength of the material. There is high possibility of existence of combination of both hydrophobic and hydrophilic nature in the same nano-structure which can alter the properties of water differently confined in it. Therefore, a model system with varied hydrophilicity and hydrophobicity may help in achieving desirable ordering and retention of water molecules in confined region or on its surface/interface. The know-how gained from such model system will further allow designing nanostructures with desirable properties and better understanding of the process of structuring of water. The design and mor-

† Electronic Supplementary Information (ESI) available: [Distribution of q_{order} is given at 1 atm and different temperatures for different regions (Fig. ESI1). θ_{ij} in q_{order} is plotted as a function of time for different regions at different temperature in Fig. ESI2. Plot for variation of average nonbonded potential energy as a function of time is provided (Fig. ESI2). Peak height of potential energy distribution at different temperature is given in Fig. ESI4]. See DOI: 10.1039/b000000x/

[a] *Physical Chemistry Division, National Chemical Laboratory, Pune-411008, India. Fax: +91 (020) 25902636; Tel: +91 (020) 25902735; E-mail: pr.pandey@ncl.res.in*

phology of the model can further be varied to approach closer to a real system. Designing such a model with incremental changes will further facilitate designing and understanding smart materials with *a priori* knowledge of the parameters to achieve desirable structuring and retention.

For organisms living in extremely cold conditions (below freezing point of water) freezing of water inside the cells can be life threatening. They withstand such drastic conditions by inhibiting freezing of water and hence ice formation by the use of some antifreeze proteins [15]. Lyophilization is a widely used technique for preservation in pharmaceutical industry [16]. This process involves freezing, followed by drying of the material for preservation. However, during the process of freezing, ordering of water molecules is capable to damage the material. In the above examples structuring of water in ordered fashion near nano-structures is the fundamental aspect to address. Thus learning from nature is may be the best way to design nano-structures with desired properties.

Extending our previous work on wettability of rough hydrophilic surfaces [17], in the present study we have designed a model system consisting of linear protrusions having hydrophobic and hydrophilic blocks. We have added the water molecules on top of the hydrophilic blocks, and investigated the structuring of water molecules near these linear atomistic protrusions for a wide range of temperatures and pressures. The model system studied here, with hydrophobic and hydrophilic blocks, and water on top of the hydrophilic blocks, is motivated from lipid bilayer-water like systems structurally, where the solute due to the presence of hydophilic head groups and hydrophobic tails self assembles as a lamella with its hydrophilic groups pointing towards water. Model systems having structural resemblance with a real system may prove to be a guide for designing smart materials. However, in the present study we have not drawn any comparison between the model nano-structure and any real lipid bilayer like systems. The protrusions are constructed of LJ particles. Hydrophilicity and hydrophobicity of the protrusions are controlled by controlling the σ and ε of the LJ-particles forming the protrusions (see Computational Methods). We have studied the local structuring, ordering and energetics of water at various positions near to the model atomistic protrusions at different temperatures and pressures keeping the position of the protrusions fixed. Temperature is varied from 290K to 200K in steps, and starting from 270 K, pressure is varied from 1 bar to 200 bar. Such variation in temperature and pressure is performed to understand the effect of high pressure, and low temperature on the structuring and retention properties of water near the model nano-structure presented in this study. We have shown in our previous study, that wettability of rough hydrophilic surfaces can vary depending upon its roughness, and surface-water non-bonded potential energy [17]. Systematic study of such model systems and further implementation of these in experimental synthesis of nano-structures would help in preparing new smart materials with tunable water retention and ordering.

2 Computational Method

2.1 The Model

The structure of the protrusion is constructed as linear with one hydrophobic and one hydrophilic block (Fig. 1). The hydrophobic block contains only one kind of particle (Hb). But, the hydrophilic block contains two kinds of particles (Hln and Hlp). The hydrophobic Hb-particles do not bear any charges.

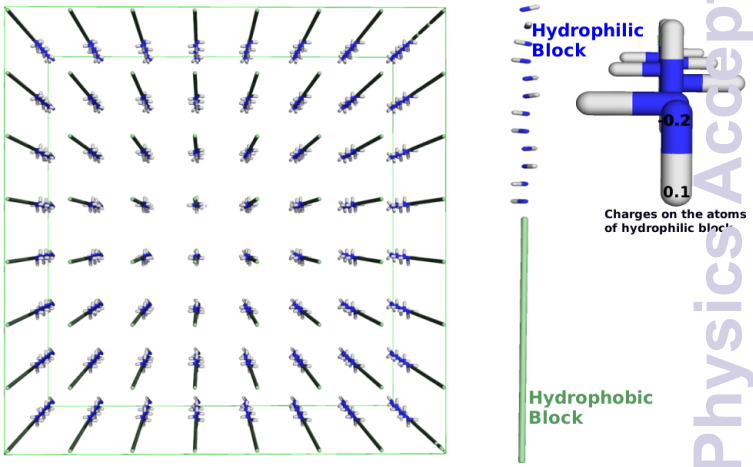

Fig. 1 The model protruded system. Individial protrusions contain one hydrophilic (blue), and one hydrophobic block (green). Hydrophobic block contains Hb-type particles (green), and hydrophilic block contains negatively charged Hln (blue) and positively charged Hlp (white) type particles. Hlp-type particles point out radially in space from protrusion. Protrusions are multiplied in the XY-plane.

Hydrophobic Hb-type particles are joined one over other along the Z-axis to construct the hydrophobic block. This is followed by the hydrophilic Hln-type particles in the same direction to form the hydrophilic block. This, as a whole, gives a linear protruded structure (Fig. 1). In addition to this, one Hlp-type particle is attached to each of the Hln-type particles in the hydrophilic block. The Hlp-type particles are arranged in the coordinate space such that they radially point outwards from the hydrophilic block (Fig. 1). This may enhance ordering of water molecules because of its inherent symmetry around the protrusions. Each of the Hlp-type (hydrophilic positively charged) particles bear a charge of +0.1 and alternate Hln-type (hydrophilic negatively charged) particles bear -0.2 (Fig. 1). This makes each of the protruded structure neutral as a whole. Finally, the protrusions were arranged along the

XY-plane (8×8) to give 64-protrusions in total (Fig. 1). A distance of 0.8 nm has been maintained between the protrusions in the starting structure throughout the XY-plane.

The model system contains distinct hydrophobic and hydrophilic regions along the Z-direction made up of the hydrophobic and hydrophilic blocks present in each of the individual protrusions. The hydrophobicity or hydrophilicity of individual particles are maintained by tuning the Lennard-Jones (LJ) interaction parameters, i.e., σ and ε for each type of particle. The σ and ε values for Hb and Hln-type particles were considered by comparing force field parameters (non-bonded LJ) of different types of atoms (hydrophobic and hydrophilic) and finally by plotting inter-particle LJ potentials, which is,

$$V_{ij} = 4\varepsilon_{ij}\left[\left(\frac{\sigma_{ij}}{r_{ij}}\right)^{12} - \left(\frac{\sigma_{ij}}{r_{ij}}\right)^{6}\right] \quad (1)$$

where r_{ij} is the distance between i and j^{th} particle.

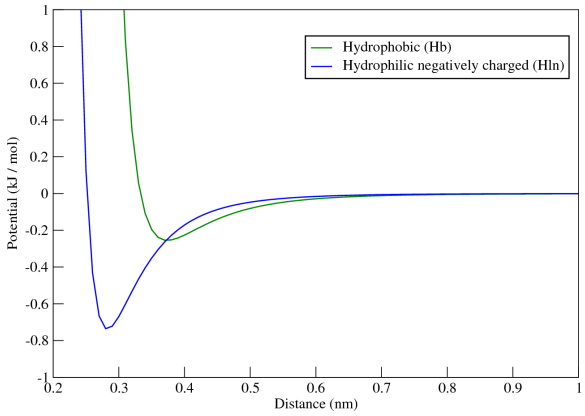

Fig. 2 LJ potential plot between Hb and Hln-type particles, and oxygen of SPC/E water.

Non-bonded interactions i.e. LJ potentials between Hb and Hln with oxygen (O) of water are shown in Fig. 2. Here r_{ij} is the distance between water O and the particle (Hln or Hlp), and σ_{ij} and ε_{ij} are determined by the combination rules $\sigma_{ij} = \sqrt{\sigma_{i(watO)}\sigma_{j(Hlb/Hln)}}$, and $\varepsilon_{ij} = \sqrt{\varepsilon_{i(watO)}\varepsilon_{j(Hlb/Hln)}}$. It is evident from Fig. 2 that the LJ-potentials for the hydrophobic and the hydrophilic particles differ in both σ and ε. Much lower values of σ and ε for the hydrophilic Hln-type particles makes their interaction with water more favorable than the hydrophobic Hb-type particles. The LJ-parameters used in the present study are listed in Table 1. σ and ε for the Hlp-type particles are 0, but they bear a positive charge (Table 1). Charges on other particles forming the protrusions are also listed in Table 1. In addition to this, σ, ε, and charges of the SPC/E water model[18] are also given in Table 1.

Table 1 List of the nonbonded parameters used for the protrusions and water.

Particle	σ (nm)	ε (kJ/mol)	q (e)
Hb	0.35	0.1	0.0
Hln	0.2	0.8368	-0.2
Hlp	0.0	0.0	0.1
Water O	0.3165	0.6501	-0.8476
Water H	0.0	0.0	0.4238

Protrusion–protrusion, water–water, and water–protrusion non-bonded interactions were taken care of using the following relation

$$V_{nonbonded} = V_{LJ} + V_{coulomb} \quad (2)$$

where $V_{coulomb}$ is the Coulomb interaction potential.

Water was added on the top of hydrophilic region of the protrusions in the initial structure (Fig. 3), such that, protrusion-water interface was created along the Z-axis. Positions of all the protrusion particles were restrained during the simulations. Water, being free to move, enters inside the hydrophilic region.

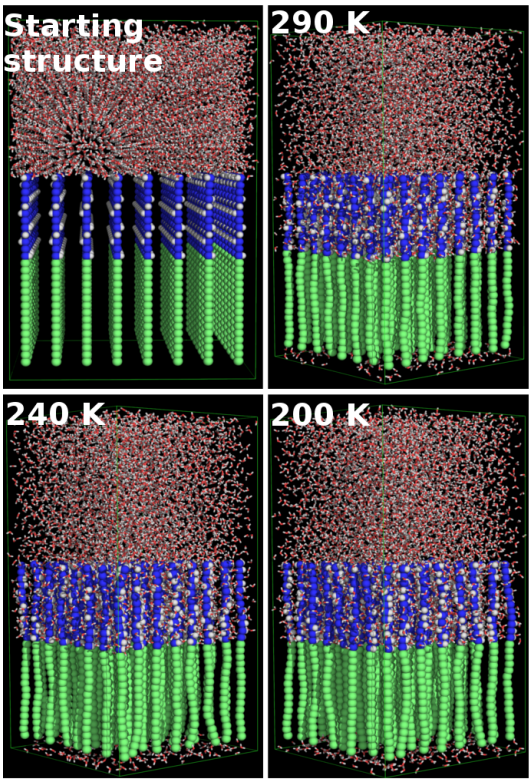

Fig. 3 Snapshots of the system at different temperatures and 1 bar.

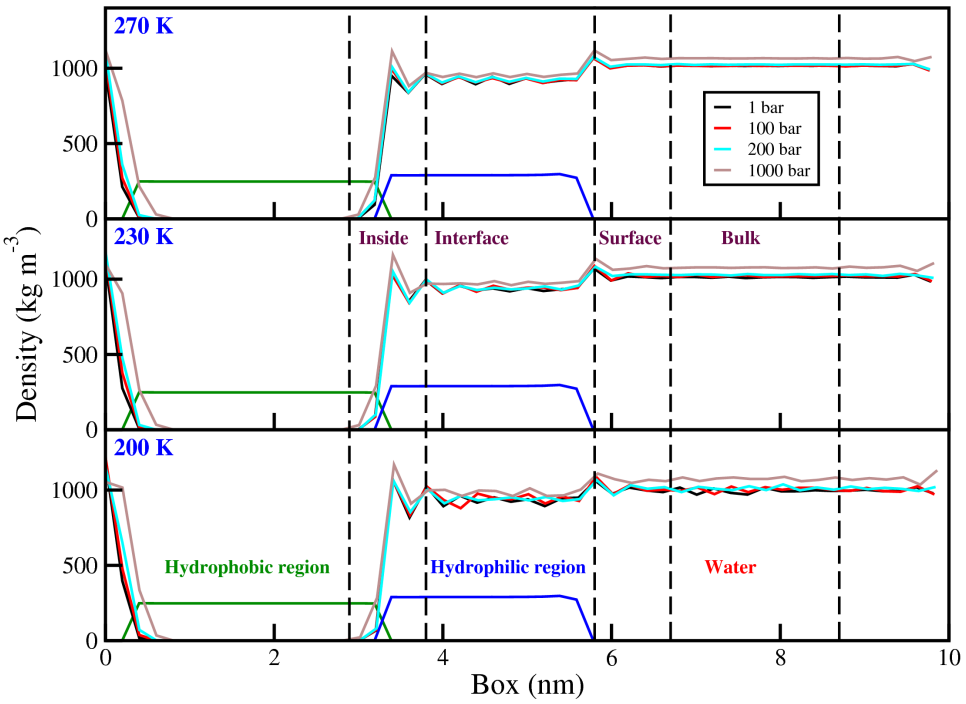

Fig. 4 Partial density of water and protrusions along Z-axis (axis perpendicular to the protrusion-water interface). Different regions are defined depending upon density of water.

2.2 Details of Simulations

All the simulations were performed using gromacs-4.5.5 package[19]. For both LJ and coulombic interactions cut off distance of 1.0 nm was applied. Long range electrostatic interactions were treated with particle mesh Ewald (PME) method[20,21]. The initial system (Fig. 3) was allowed to equilibrate at 290 K and 1 bar for 10 ns. Then a production run of 10 ns was performed and analyzed further. Finally, the temperature was decreased slowly in steps of 10 K upto 200 K by taking the output structure at each temperature as an input for the next lower temperature. 20 ns simulations were performed at each temperature. We have checked the average potential energy in different regions of the system as a function of time (discussed in section 3.2) to confirm that the system is equilibrated. The protrusions were position restrained, as implemented in gromacs-4.5.5, in all the simulations. This process of cooling allowed the water molecules to penetrate more inside the hydrophilic region. In addition to this, 20 ns simulations were also performed at higher pressures from 270 to 200 K temperatures. Simulations were performed at 1, 200, 100, and 1000 bar pressures. 1000 bar pressure was studied to check the effect of such high pressure on structure and dynamics of water molecules. All the simulations were performed using isothermal-isobaric (NPT) ensemble. V-rescale thermostat[22] and Berendsen barostat[23] was used to keep the temperature and pressure constant respectively. Semi-isotropic pressure coupling in XY- and Z-directions and periodic boundary condition (PBC) were applied in all the simulations.

3 Results

Water-protrusion interface was created along Z-axis in the initial structure (Fig. 3), and water was allowed to interact with the protrusions. No water molecules were present inside any regions of the protrusions in the initial structure. During the equilibration at 290 K and 1 bar water enters inside the hydrophilic region of the protrusions (Fig. 3). Further, as the temperature is decreased at 1 bar water molecules move deeper inside the hydrophilic region, upto the starting of hydrophobic region (Fig. 3). Protrusions, being position restrained in all the simulations i.e., fluctuates around mean positions, the hydrophilic and hydrophobic regions are well defined in all the simulations. Further, to quantitatively understand upto what point water enters inside the hydrophilic region, partial density of water along Z-axis (direction of protrusion-water interface) is calculated and shown in Fig. 4. At a particular temperature partial density of water is shown for different pressures (Fig. 4). Since the position of protrusions are fixed in all the simulations, only one partial density is shown for them. The partial densities for hydrophilic, and

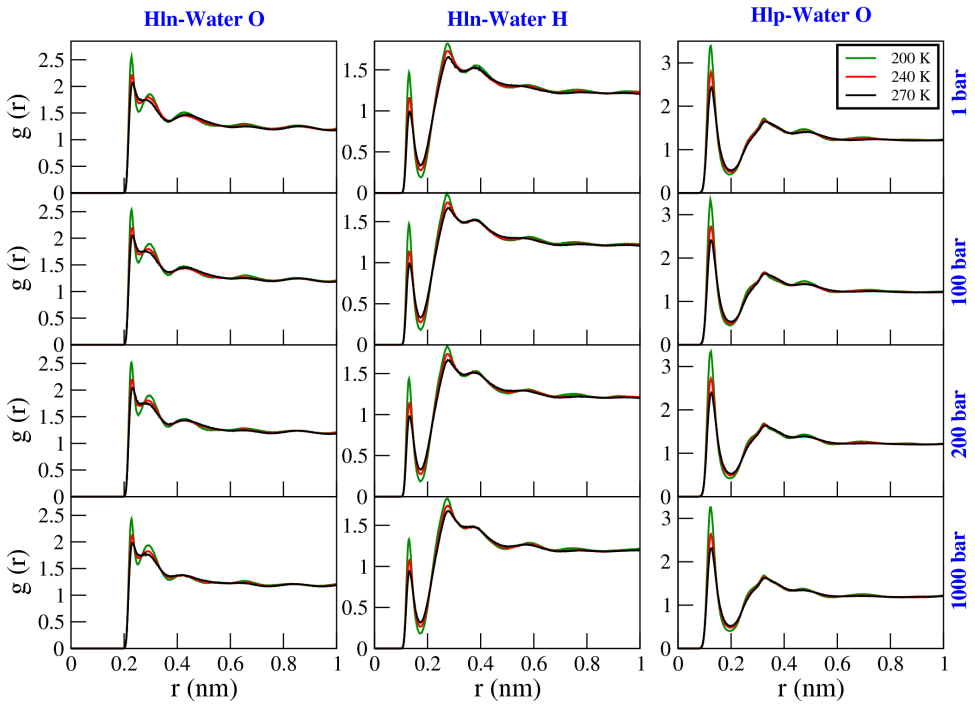

Fig. 5 RDF between water and different particles of protrusions.

hydrophobic regions are shown distinctly. At a particular temperature, water enters more deeper inside the protrusions as the pressure is increased. At 270 K and 1 bar water penetrates upto the junction of hydrophobic and hydrophilic regions, but at 1000 bar the water molecules seem to move inside the starting of the hydrophobic region. This level of penetration upto the hydrophobic region keep increasing gradually on moving from 1 bar to 1000 bar. Similar gradual increase can be observed at 230, and 200 K also. At all these temperatures and pressures water molecules are wetting the hydrophilic region because of choice of attractive LJ potentials and electrostatic interaction. These interactions are further quantified in section 3.2. Few water molecules are present near the end hydrophobic region (Hb-type) i.e., near 0-1 nm due to periodic boundary condition along Z-axis.

Depending upon density of water we have defined four regions along the Z-axis: inside (2.8–3.8 nm), interface (3.8–5.8 nm), surface (5.8–6.7 nm), and bulk (6.7–8.7 nm). In the inside region, water is closest to the hydrophobic region of protrusions and water density keeps on increasing and almost touches 1000 kg m^{-3} in this region. The region starting from the end of the inside region and ending at the end of hydrophilic region has been defined as the interface region. The density of water fluctuates around 1000 kg m^{-3}. Further, a small block just above the hydrophilic protrusions where the density of water continues to fluctuate is defined as the surface region. Water molecules in this region are closest to the protruded hydrophilic surface. Fluctuations in water density and structuring of water molecules near hydrophobic surfaces, and have been studied in the past[24–26]. Thus it is interesting to understand such phenomenon near the hydrophilic surface formed by the hydrophilic region of the protrusions. Finally, the region with almost same density (less fluctuation) is defined as the bulk. We have analyzed and distinguished the differences in structuring and energetics of water in these regions separately.

3.1 Ordering of Water Molecules

3.1.1 Ordering of Water Molecules Near Protrusions

Water molecules penetrate the hydrophilic region because of favourable interaction potential. The Hlp particles point radially outward from the hydrophilic region of the protrusions. This may support the ordering of water molecules near the protrusions. Radial distribution function (RDF) plots are shown in Fig. 5 at different temperatures at a particular pressure to understand the ordering of water molecules around Hln and Hlp-type particles present in the hydrophilic region of protrusions. The peak heights of all the RDF plots increase with decrease in temperature at one pressure. This indicates more ordering of water molecules near the Hln and Hlp-type particles with decrease in temperature. For all the RDFs between particle Hln and water O a sharp first peak at 0.23 nm is

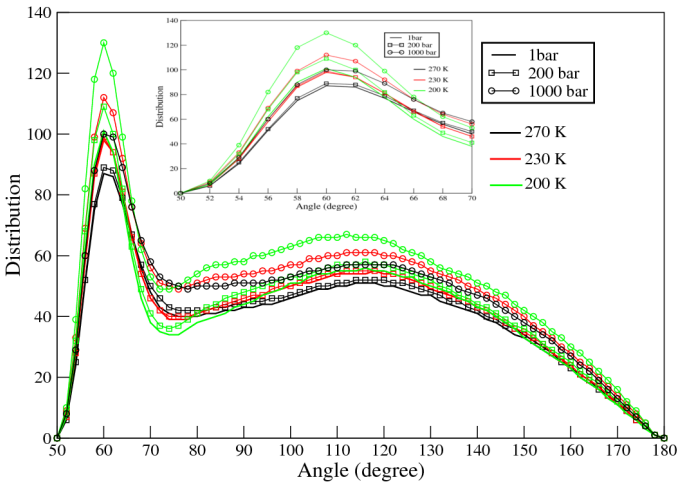

Fig. 6 Distribution of the angle between water O, particle Hln, and water O. The first peak is focussed in the inset.

present at all the temperatures and pressures. A second peak gradually forms with decrease in temperature at a particular pressure. This indicates that though the water molecules order near the Hln-type particles, the ordering is translated further in the second solvation shell with decrease in temperature. This is more evident from the RDFs between particle Hln and water H. There are two distinct peaks at all temperatures and pressures indicative of two solvation shells and the peak heights of both the peaks increase with decrease in temperature. This shows increase in ordering of water molecules in both the solvation shells with decrease in temperature. The first peak height, corresponding to first solvation shell, in the RDF between particle Hlp and water O also increases with decrease in temperature at all pressures. Though there is not much change in the second peak.

Further, to construe the overall picture of ordering of water molecules near the protrusions, distribution of angles between water O, Hln-type particle, and water O (O-Hln-O) is calculated and shown in Fig. 6. For calculating these distributions, first, all the water molecules falling within a distance of 0.4 nm (corresponding to minima of second peak of particle Hln-water O RDF in Fig. 5) from the Hln-type particles, which have more than two water molecules as its neighbour, were identified. Then, the O-Hln-O angle was computed for all such water molecules, and the angles were converted into a histogram. Finally, the distributions were plotted for all sets of simulations and normalized over the number of frames present in the last 2 ns of the trajectories. Two distinct peaks can be observed at all the temperatures and pressures (Fig. 6). The second peak is comparatively broader than the first. At a particular temperature, peak heights increases with increase in pressure. Not much difference in peak height is observed for 1 bar and 200 bar pressures at a particular temperature, but at 1000 bar peak height is the highest (first peaks are zoomed in the inset of Fig. 6). Also, peak height increases on decreasing temperature. This is in correspondence with the peak heights of RDF plots, and indicate higher ordering at lower temperatures. The first peak near 60° suggests that a particular orientation of water molecules near the protrusions is favoured. Broad second peak of O-Hln-O angle distribution may have been caused by the water molecules residing in the second solvation shell. Ordering of water molecules present in the second solvation shell experience less attraction from Hln and Hlp-type particles because of shielding by the first solvation shell as well as water-water interactions may get favoured. However, water molecules inside the hydrophilic region experience interaction from Hln and Hlp-type particles and favours ordering near to the nearest protrusions.

3.1.2 Water–Water Ordering In addition to ordering of water molecules involving the particles of protrusions at the interface region, it is also important to investigate the structuring of water molecules at the surface and bulk region due to the presence of protrusions. Orientational order parameter[27] (q_{order}) is calculated to understand such water-water ordering. It is defined as

$$q_{order} = 1 - \frac{3}{8}\sum_{i=1}^{3}\sum_{j=i+1}^{4}\left(\cos\theta_{ij} + \frac{1}{3}\right)^2 \qquad (3)$$

where θ_{ij} is the angle between the vectors joining the oxygen atom of one water molecule and oxygen atom of its nearest neighbour water molecules i and $j(\leq 4)$. Distribution of q_{order} at different pressures at particular temperature is shown in Fig. 7. q_{order} signifies the extent by which four nearest neighbours assemble in a tetrahedral configuration[27]. For a perfect tetrahedral arrangement $q_{order} = 1$, and $q_{order} = 0$ for random arrangement. q_{order} has been calculated in the past for water molecules confined inside hydrophobic, hydrophilic, and heterogeneous plates by Giovambattista et al[28]. Thus, calculation of q_{order} is relevant to understand the water-water ordering in different regions defined in Fig. 4. q_{order} per water was calculated first for each region separately and converted into histogram. Finally, distributions are plotted normalizing over total number of frames in last 2 ns for all the trajectories (Fig. 7).

The peaks of the distributions can clearly be seen to be shifting towards higher q_{order} value with decrease in temperature (Fig. 7). Higher q_{order} value indicates higher tetrahedral ordering, so it is somehow obvious that water molecules are more tetrahedrally ordered at low temperatures. For a temperature q_{order} is lower for 1000 bar with respect to 1, 100, and 200 bar pressures. Although, even at 1000 bar q_{order} increases on lowering the temperature.

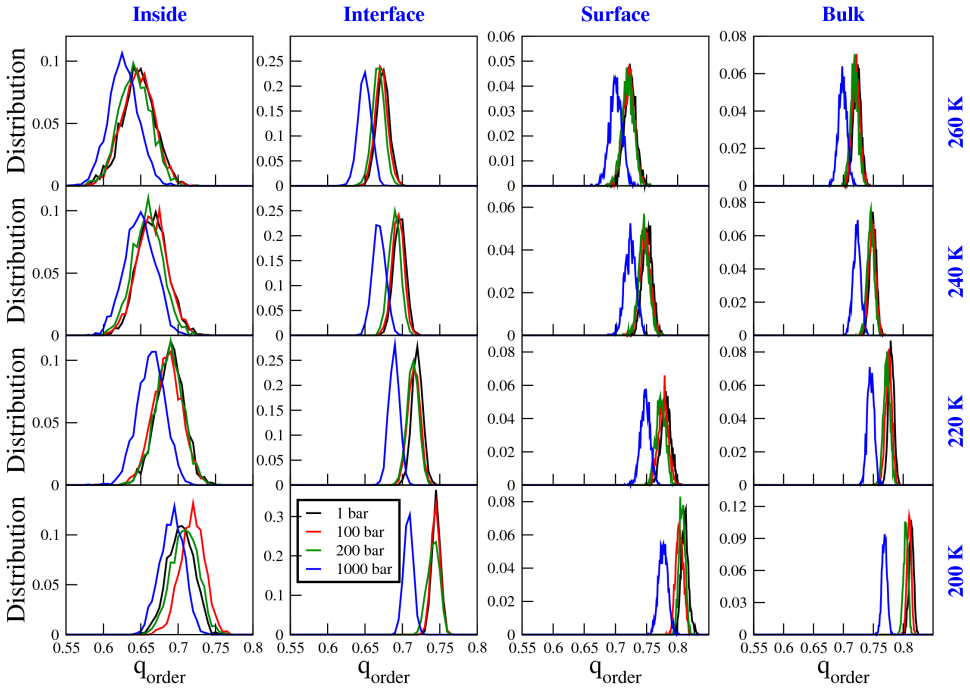

Fig. 7 Distribution of order parameters calculated for different regions at different temperatures and pressures.

Distributions of q_{order} for inside region is broader than interface, surface, and bulk. This fact is evident from the the q_{order} distributions shown in Fig. ESI1 at 1 bar and different temperatures. It suggests that at a temperature the q_{order} value varies as inside $<$interface $<$surface $\simeq$ bulk. This is because, in the inside region water molecules are nearest to the hydrophobic Hb-type particles. Due to the unfavourable interactions with the Hb-particles inside region water molecules deviate more from tetrahedral arrangement (lower q_{order} value). Also, plot of average θ_{ij} as function of time given in Fig. ESI2 shows higher fluctuation for inside region. This accounts for the broadness of the q_{order} plot for inside region (Fig. 7 and Fig. ESI1). From the RDF (Fig. 5) and angle distribution (Fig. 6) we have seen that water molecules are ordered near the protrusion and the interactions between protrusion particles and water molecules may facilitate the departure from tetrahedral ordering. Water molecules present in the interface region are nearest to the Hln- and Hlp-type particles. But at the same time they feel the unfavourable hydrophobic interactions of Hb-type particles. As a result, distribution of q_{order} for the interface region appear at higher value than inside region Fig. (7 and Fig. ESI1). The nonbonded interactions are quantified in section 3.2. Surface region water molecules are closest to surface formed by the hydrophilic particles of the protrusions. They face least unfavourable hydrophobic interactions with the Hb-type particles as they are farther, and also due to screening by the inside and interface region water molecules. Higher ordering in the surface region accounts for the fluctuations in density observed (Fig. 4).

3.2 Energy Profiles for Different Regions

Higher ordering can also be related to favourable potential energy. Therefore, it is important to check whether the tetrahedrally ordered surface or ordered (but less tetrahedrally) interface water molecules are at the lower potential energy than other regions. Therefore total non-bonded interactions per water molecule is computed and plotted for each region in Fig. 8. It represents the average total non-bonded potential felt by individual water molecules present in a particular region. The non-bonded interactions experienced by each water molecule present in any region are sum of van der Waals and Coulombic interaction among water molecules, and between water protrusions particles. The total non-bonded interaction potential energy is calculated as the sum of LJ and Coulomb. The LJ potentials were calculated using equation 1 for the pair of particles concerned. Coulombic potentials were computed as $q_i q_j / 4\pi\varepsilon_\circ r_{ij}$, where q_i and q_j are the charges on the concerned atoms and r_{ij} is the distance between them, and $\varepsilon_\circ$ is the permittivity of vacuum. The term ε_r (permittivity of the medium) was taken as 1 in all the simulations. The term $1/4\pi\varepsilon_\circ$ is equal to 138.935485 kJ mol^{-1} nm e^{-2}. Though we have used PME electrostatics in all our simulation, calculation of coulombic interactions in this way gives the exact electro-

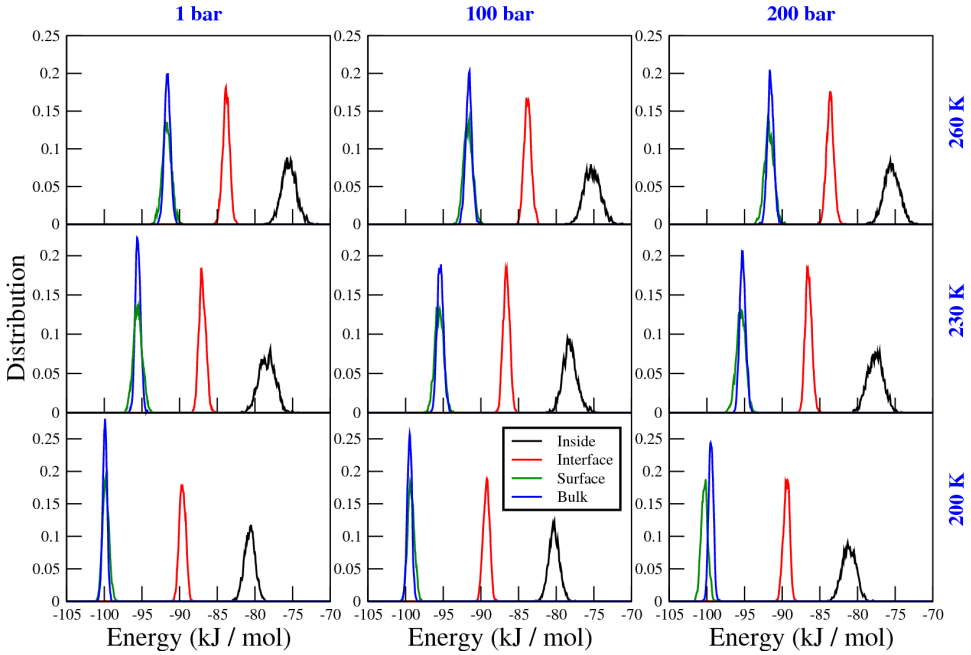

Fig. 8 Distribution of average total non-bonded potential energy.

static potential experienced by each water molecule present in a region. The water molecules present in each region (see Fig. 4) were tagged in each frame. The sum of LJ and Coulombic potentials was computed for each water molecule in all the regions separately due to all the other particles present in the system for each frame and averaged over the number of water molecules corresponding to each region separately. This gave the average non-bonded potential energy per water molecule in each frame for different regions separately. These non-bonded energies as a function of time is provided in the † ESI (Fig. ESI3) for last 2 ns of trajectory. Finally, the average non-bonded potential energy per water molecule was converted into a histogram which is further normalized by the number of frames in last 2 ns (see Fig. 8). It is evident from the plots that at almost all the temperatures and pressures the value of average non-bonded potential energy per water molecule is the least for the surface and bulk regions, and the most for the inside region. The water molecules of the inside region are closest to the hydrophobic region and contribute to repulsive interaction. But the water molecules present in the surface region are interacting more with the particles of the hydrophilic region and less with hydrophobic particles, which in total promotes attractive interaction. This is consistent with the order of q_{order} parameters for the different regions see Fig. 7, and Fig. ESI1). That is higher ordered region shows lower potential energy.

The water molecules at the surface region are experiencing the attractive hydrophilic interactions due to the protrusion particles and at the same time gaining stability by tetrahedral ordering. As a function of temperature the change in position of peaks (Fig. 8) is noticeable. This is more evident from the plot of peak height of potential energy distribution at different temperatures (Fig. ESI4). Potential energy can be clearly seen to be decreasing with decrease in temperature. This drop is also visible with variation in pressure.

3.3 Residence Time

Survival probability of water molecules present in different layers of lipid bilayer-water system was calculated in the past by Debnath et al.[29]. They represented the probability of a water molecule to stay in a layer for certain duration of time. In our system we have distinct regions and observed differences in potential energy experienced by water molecules at different regions (see Fig. 8). Thus residence time of water molecules in different regions can provide useful information about the favourable regions for water molecules to stay longer which eventually can be correlated to the probability of water retention. The residence time distribution, i.e., duration upto which a water molecule resides in a particular region (Fig. 4), is calculated and its distribution is shown in Fig. 9 i.e., the time is plotted with respect to its occurrence (Fig. 9). All the simulations were extended for 1 ns because of expected longer residence time and the coordinates of all the atoms were saved every 10 fs (referred as condensed trajectory) for this calculation. For calculating the time of con-

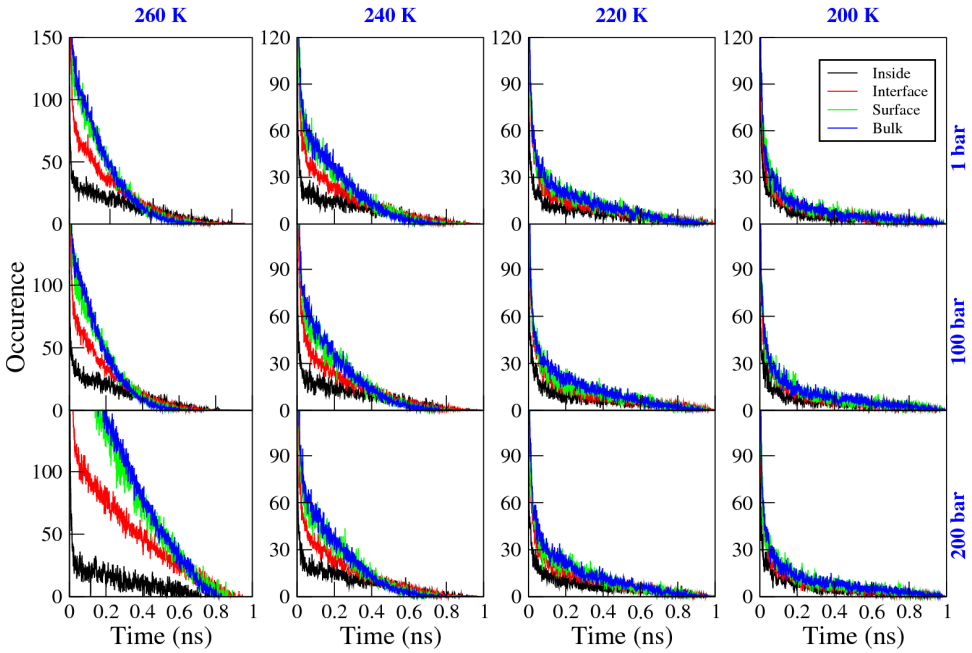

Fig. 9 Residence time distribution for water molecules in different regions.

tinuous stay, each region defined in Fig. 4 is further divided into small slabs of width 0.35 nm (the minima of first peak of O-O RDF of water comes near 0.32 nm) along z-axis. Then, the water molecules present in these slabs were identified in each frame of the condensed 1 ns trajectories. 0.32 nm of slab width was considered along with a soft boundary of 2 ps time for the calculation. This implementation of the soft boundary (as time) to make sure that, if a water molecules move out from a slab and again comes back to the same slab within 2 ps, we considered it to be present in that slab continuously [30]. This is because in 2 ps water molecules can not drift away to a large distance from the slab which makes the boundaries of the slabs much coarser. The soft boundary was also used by Impey et al. [31] to calculate the residence time of water molecules in the first solvation shell of ions. Finally, the occurrence as a function of time is depicted in Fig. 9 for all temperatures and pressures. The occurrences are represented for different regions (Fig. 4) separately, and are averaged over all the slabs of a certain region.

The residence time distribution for bulk and surface region at high temperatures (260 K) and low pressures (1 bar) is almost same. However at all temperatures and pressures the residence time distribution decays faster in the interface and inside regions than surface region indicating fast and slow dynamical motions of water molecules. Lower residence time for inside region water molecules may attributed to the hydrophobic repulsion from the hydrophobic particles which drives out the water molecules towards the interface region, and there is a fast exchange happening between these two regions. Additionally, the interface region is energetically favourable (refer Fig. 8) as compared to inside region, which supports the longer stay of water molecules in this region hence the longer residence time distribution with respect to inside region. Also, water molecules in the surface region are more tetrahedrally oriented than the inside and interface region water molecules (Fig. 7 and Fig. ESI1). This contributes to the higher residence time for water molecules present in surface region as compared to inside and interface regions. Because higher ordering implies hopping motion of water between different sites which may result into lesser exchange with other regions. Thus there might be a competition between ordering and energetics to guide the residence time of water. At 260 K, residence time is more for the inside region than the surface region. Here, energetics guides the ordering. But, as the temperature is lowered ordering starts to guide the residence time. That is why at 200 K surface region water molecules have higher residence time than that of inside region.

Further, the residence time plots (Fig. 9) were fitted with a bi-exponential function of the form

$$y = a_f exp(-\frac{t}{\tau_f}) + a_s exp(-\frac{t}{\tau_s}) + a_0 \quad (4)$$

where τ_f and τ_s are the fast and slow relaxation times respectively, and a_f and a_s are the respective amplitudes [29,30]. The fitted plots for different regions at different temperatures and pressures are provided in Fig. ESI5. Higher value of τ_f or τ_s

represent slower relaxation and hence slower dynamics. Table containing values of τ_f, τ_s, a_f and a_s for different regions at different temperature and pressure are provided in ESI. The values are higher as compared to the values reported in references [29] and [30] as the temperatures at which residence times are calculated are lower in the present study. Also the definition of the regions to calculate the survival probability are different. They are computed with respect to their motion along z-axis in different regions. The lateral motion is not accounted for as motion of water molecules in xy-plane does not change the region (Fig. 4). τ_f is lower for the surface region as compared to the inside and interface regions (Table ESI1) for all regions at all temperatures and pressures. This indicates that the fast decaying component is lower for surface region.

4 Conclusion

The model nano-structure studied here favours structuring and retention of water molecules. The LJ particles constructing the protrusions are defined with respect to their interaction with the SPC/E water. The parameters defined are good enough to allow water molecules to penetrate inside the hydrophilic region. The main advantage of the model is the penetration of water molecules can be enhanced just by tuning the parameters of the protrusions. The main limitation of the model is the protrusions are position restrained so the high flexibility of the surface atoms are not considered. This may lead to some amount of discrepancies in the results.

In our previous study, we have investigated the effect of roughness, and non-bonded interaction parameters on wetting of hydrophilic surfaces [17]. In the present study, we have diversified the model system to understand the effect of both hydrophobic, and hydrophilic particles on structural and dynamical properties of water. The knowledge gained from these model systems can be helpful in designing smart materials that can retain water inside them. The residence time of water molecules is atleast 100 ps in any region at different temperature and pressure (Fig. 9). Such retention can also be acheived for solvents other than water by just tuning the parameters of protrusions. Also, the residence time of water molecules can be further increased by increasing the hydrophilicity or decreasing hydrophobicity of the particles of protrusions. However, as a model system this is one of the first approach to rationally design such atomic protrusion water interface which can address many fundamental questions related to ordering and retention of water molecules.

In this work MD simulations were performed over a range of temperatures and pressures. Initially, no water molecules were present inside the protrusions. The water molecules penetrate the hydrophilic region of the protrusions. This penetration has been quantified by plotting the partial densities (Fig. 4) which also helped us designating different regions. We have observed tetrahedral ordering of water molecules in the surface region. Water molecules experience favourable potential energy in the interface region due to the hydrophilic environment. The water molecules at the surface region are also experiencing favourable potential energy which facilitate the tetrahedral ordering. From the residence time of water molecules it is clear that there are faster and slower motion of water molecules residing in the inside and surface regions due to balance between hydrophobic repulsion from protrusion particles (inside region) and favourable (energetically) interface region.

The ice-water transition (melting) for SPC/E water model has been reported to be taking place near 213 K [32]. In our simulations with the model protrusions, we have not observed any ice formation. Though the ordering of water molecules increase at lower temperatures (Fig. 7), we did not observe any ice formation. It has been reported in the past that water in its supercooled state can have large value of order parameters, but it does not necessarily mean ice formation [33,34]. The nucleation and growth of ice involves an energy barrier to be crossed. Also, in the present model system the different LJ particles may favour or hinder the ice nucleation. This is an important issue to be addressed. Because at very low temperatures ice formation in the hydrophilic region of lipid bilayer may rupture it. Also, ice formation inside the hydrophilic grooves can be a challenge for the lyophilization [16] process as it can damage the structure of the material. Thus, understanding the structuring, and growth of ice inside the atomistic model protrusions discussed here would better equip us to deal with the problems in the real systems. But, the main challenge to such study is the nucleation of ice in molecular dynamics time scale.

The model system studied here is the first step in designing smart materials having water retention capability. Being an atomistic model it helps to understand the ordering of water molecules at the structural level. Such a structural level insight can be the basis to understand structuring of water in the real systems. The atomistic model can be further extended to structured models in the future keeping the hydrophilic, and hydrophobic blocks intact. The parameters can also be tuned to get desired properties. In addition to this, ice formation and growth inside the nano confined region formed by the protrusions can also be studied further.

Acknowledgement: We gratefully acknowledge CSIR and NCL for financial support for the project. Author SR gratefully acknowledges DST (Project code SB/S1/PC-069/2013) and center for excellence in scientific computing, NCL, for financial support and computational time. Author PRP acknowledges Mr. Chandan Kumar Choudhury for insightful discussions regarding implementation of soft boundary in the residence time calculation.

References

1 J. C. Rasaiah, S. Garde and G. Hummer, *Annu. Rev. Phys. Chem.*, 2008, **59**, 713–740.
2 R. Mancinelli, *J. Phys.: Condens. Matter*, 2010, **22**, 404213.
3 D. Takaiwa, I. Hatano, K. Koga and H. Tanaka, *PNAS*, 2008, **105**, 39–43.
4 M. D. Collins, G. Hummer, M. L. Quillin, B. W. Matthews and S. M. Gruner, *PNAS*, 2005, **102**, 16668–16671.
5 M. D. Collins, M. L. Quillin, G. Hummer, B. W. Matthews and S. M. Gruner, *J. Mol. Biol.*, 2007, **367**, 752 – 763.
6 S. Vaitheeswaran, H. Yin, J. C. Rasaiah and G. Hummer, *PNAS*, 2004, **101**, 17002–17005.
7 S. Vaitheeswaran, J. C. Rasaiah and G. Hummer, *J. Chem. Phys.*, 2004, **121**, 7955–7965.
8 Y. Leng and P. T. Cummings, *Phys. Rev. Lett.*, 2005, **94**, 026101.
9 K. Koga and H. Tanaka, *J. Chem. Phys.*, 2005, **122**, 104711.
10 J. C. Johnston, N. Kastelowitz and V. Molinero, *J. Chem. Phys.*, 2010, **133**, 154516.
11 S. Khan and J. K. Singh, *Molecular Simulation*, 2013, **0**, 1–11.
12 H. Kumar, B. Mukherjee, S.-T. Lin, C. Dasgupta, A. K. Sood and P. K. Maiti, *J. Chem. Phys.*, 2011, **134**, 124105.
13 T. G. Lombardo, N. Giovambattista and P. G. Debenedetti, *Faraday Discuss.*, 2009, **141**, 359–376.
14 B. A. Bauer, S. Ou, S. Patel and K. Siva, *Phys. Rev. E*, 2012, **85**, 051506.
15 A. L. DeVries, *Annu. Rev. Physiol.*, 1983, **45**, 245–260.
16 W. Wang, *Int. J. Pharm.*, 2000, **203**, 1 – 60.
17 P. R. Pandey and S. Roy, *J. Phys. Chem. Lett.*, 2013, **4**, 3692–3697.
18 H. J. C. Berendsen, J. R. Grigera and T. P. Straatsma, *J. Phys. Chem.*, 1987, **91**, 6269–6271.
19 S. Pronk, S. Pll, R. Schulz, P. Larsson, P. Bjelkmar, R. Apostolov, M. R. Shirts, J. C. Smith, P. M. Kasson, D. van der Spoel, B. Hess and E. Lindahl, *Bioinformatics*, 2013, **29**, 845–854.
20 D. Frenkel and B. Smit, *Understanding Molecular Simulation: From Algorithms to Applications*, Academic Press, Inc., Orlando, FL, USA, 2nd edn., 2002.
21 M. P. Allen and D. J. Tildesley, *Computer Simulation of Liquids*, Clarendon Press, Oxford, 1987.
22 G. Bussi, D. Donadio and M. Parrinello, *J. Chem. Phys.*, 2007, **126**, 014101.
23 H. J. C. Berendsen, J. P. M. Postma, W. F. van Gunsteren, A. Dinola and J. R. Haak, *J. Chem. Phys.*, 1984, **81(8)**, 3684 – 3690.
24 F. MullerPlathe, S. Pal, H. Weiss and H. Keller, *Soft Materials*, 2005, **3**, 21–43.
25 S. Pal, H. Weiss, H. Keller and F. Muller-Plathe, *Phys. Chem. Chem. Phys.*, 2005, **7**, 3191–3196.
26 F. Leroy and F. Mller-Plathe, *Journal of Chemical Theory and Computation*, 2012, **8**, 3724–3732.
27 J. R. Errington and P. G. Debenedetti, *Nature*, 2001, **409**, 318–321.
28 N. Giovambattista, P. J. Rossky and P. G. Debenedetti, *J. Phys. Chem. B*, 2009, **113**, 13723–13734.
29 A. Debnath, B. Mukherjee, K. G. Ayappa, P. K. Maiti and S.-T. Lin, *J. Chem. Phys.*, 2010, **133**, 174704.
30 C. K. Choudhury and S. Roy, *Soft Matter*, 2013, **9**, 2269–2281.
31 R. W. Impey, P. A. Madden and I. R. McDonald, *J. Phys. Chem.*, 1983, **87**, 5071–5083.
32 R. G. Fernandez, J. L. F. Abascal and C. Vega, *J. Chem. Phys.*, 2006, **124**, 144506.
33 E. B. Moore, E. de la Llave, K. Welke, D. A. Scherlis and V. Molinero, *Phys. Chem. Chem. Phys.*, 2010, **12**, 4124–4134.
34 E. B. Moore and V. Molinero, *Nature*, 2011, **479**, 506–508.